

Minerva Access is the Institutional Repository of The University of Melbourne

Author/s:

Cui, JX;Li, YB;Shen, CP;Adachi, I;Aihara, H;Al Said, S;Asner, DM;Aushev, T;Ayad, R;Babu, V;Bahinipati, S;Banerjee, S;Bauer, M;Behera, P;Belous, K;Bennett, J;Bessner, M;Bhuyan, B;Bilka, T;Biswas, D;Bobrov, A;Bodrov, D;Borah, J;Bračko, M;Branchini, P;Browder, TE;Budano, A;Campajola, M;Červenkov, D;Chang, MC;Cheon, BG;Chilikin, K;Cho, K;Choi, SK;Choi, Y;Choudhury, S;Das, S;Dash, N;De Nardo, G;De Pietro, G;Dhamija, R;Di Capua, F;Dingfelder, J;Doležal, Z;Dong, TV;Dubey, S;Ecker, P;Epifanov, D;Ferber, T;Ferlewicz, D;Fulsom, BG;Garg, R;Gaur, V;Garmash, A;Giri, A;Goldenzweig, P;Graziani, E;Gudkova, K;Hadjivasiliou, C;Halder, S;Hayasaka, K;Hayashii, H;Hazra, S;Herrmann, D;Hou, WS;Hsu, CL;Inami, K;Ipsita, N;Ishikawa, A;Itoh, R;Iwasaki, M;Jacobs, WW;Jia, S;Jin, Y;Kalita, D;Kiesling, C;Kim, DY;Kim, KH;Kim, YK;Kinoshita, K;Kodyš, P;Korobov, A;Korpar, S;Kovalenko, E;Križan, P;Krokovny, P;Kuhr, T;Kumar, D;Kumar, R;Kwon, YJ;Lam, T;Lee, SC;Li, LK;Li, Y;Li Gioi, L;Libby, J;Liventsev, D;Ma, Y;Masuda, M;Matvienko, D

Title:

Search for the semileptonic decays $\Xi c 0 \rightarrow \Xi 0 \ell^+ \ell^-$ at Belle

Date:

2024-03-01

Citation:

Cui, J. X., Li, Y. B., Shen, C. P., Adachi, I., Aihara, H., Al Said, S., Asner, D. M., Aushev, T., Ayad, R., Babu, V., Bahinipati, S., Banerjee, S., Bauer, M., Behera, P., Belous, K., Bennett, J., Bessner, M., Bhuyan, B., Bilka, T., ... Matvienko, D. (2024). Search for the semileptonic decays $\Xi c 0 \rightarrow \Xi 0 \ell^+ \ell^-$ at Belle. *Physical Review D*, 109 (5), pp.052003-. <https://doi.org/10.1103/PhysRevD.109.052003>.

Persistent Link:

<https://hdl.handle.net/11343/351832>

License:

[cc-by](#)

Search for the semileptonic decays $\Xi_c^0 \rightarrow \Xi^0 \ell^+ \ell^-$ at Belle

J. X. Cui¹, Y. B. Li², C. P. Shen³, I. Adachi⁴, H. Aihara⁵, S. Al Said⁶, D. M. Asner⁷, T. Aushev⁸, R. Ayad⁹, V. Babu¹⁰, S. Bahinipati¹¹, Sw. Banerjee¹², M. Bauer¹³, P. Behera¹⁴, K. Belous¹⁵, J. Bennett¹⁶, M. Bessner¹⁷, B. Bhuyan¹⁸, T. Bilka¹⁹, D. Biswas²⁰, A. Bobrov²¹, D. Bodrov²², J. Borah²³, M. Bračko²⁴, P. Branchini²⁵, T. E. Browder²⁶, A. Budano²⁷, M. Campajola²⁸, D. Červenkov²⁹, M.-C. Chang³⁰, B. G. Cheon³¹, K. Chilikin³², K. Cho³³, S.-K. Choi³⁴, Y. Choi³⁵, S. Choudhury³⁶, S. Das³⁷, N. Dash³⁸, G. De Nardo³⁹, G. De Pietro⁴⁰, R. Dhamija⁴¹, F. Di Capua⁴², J. Dingfelder⁴³, Z. Doležal⁴⁴, T. V. Dong⁴⁵, S. Dubey⁴⁶, P. Ecker⁴⁷, D. Epifanov⁴⁸, T. Ferber⁴⁹, D. Ferlewicz⁵⁰, B. G. Fulsom⁵¹, R. Garg⁵², V. Gaur⁵³, A. Garmash⁵⁴, A. Giri⁵⁵, P. Goldenzweig⁵⁶, E. Graziani⁵⁷, K. Gudkova⁵⁸, C. Hadjivasiliou⁵⁹, S. Halder⁶⁰, K. Hayasaka⁶¹, H. Hayashii⁶², S. Hazra⁶³, D. Herrmann⁶⁴, W.-S. Hou⁶⁵, C.-L. Hsu⁶⁶, K. Inami⁶⁷, N. Ipsita⁶⁸, A. Ishikawa⁶⁹, R. Itoh⁷⁰, M. Iwasaki⁷¹, W. W. Jacobs⁷², S. Jia⁷³, Y. Jin⁷⁴, D. Kalita⁷⁵, C. Kiesling⁷⁶, D. Y. Kim⁷⁷, K.-H. Kim⁷⁸, Y.-K. Kim⁷⁹, K. Kinoshita⁸⁰, P. Kodyš⁸¹, A. Korobov⁸², S. Korpar⁸³, E. Kovalenko⁸⁴, P. Križan⁸⁵, P. Krokovny⁸⁶, T. Kuhr⁸⁷, D. Kumar⁸⁸, R. Kumar⁸⁹, Y.-J. Kwon⁹⁰, T. Lam⁹¹, S. C. Lee⁹², L. K. Li⁹³, Y. Li⁹⁴, L. Li Gioi⁹⁵, J. Libby⁹⁶, D. Liventsev⁹⁷, Y. Ma⁹⁸, M. Masuda⁹⁹, D. Matvienko¹⁰⁰, S. K. Maurya¹⁰¹, F. Meier¹⁰², M. Merola¹⁰³, K. Miyabayashi¹⁰⁴, R. Mizuk¹⁰⁵, R. Mussa¹⁰⁶, M. Nakao¹⁰⁷, Z. Natkaniec¹⁰⁸, A. Natochii¹⁰⁹, L. Nayak¹¹⁰, S. Nishida¹¹¹, S. Ogawa¹¹², H. Ono¹¹³, P. Oskin¹¹⁴, P. Pakhlov¹¹⁵, G. Pakhlova¹¹⁶, S. Pardi¹¹⁷, H. Park¹¹⁸, J. Park¹¹⁹, S.-H. Park¹²⁰, S. Patra¹²¹, S. Paul¹²², T. K. Pedlar¹²³, R. Pestotnik¹²⁴, L. E. Piilonen¹²⁵, T. Podobnik¹²⁶, M. T. Prim¹²⁷, N. Rout¹²⁸, G. Russo¹²⁹, S. Sandilya¹³⁰, L. Santelj¹³¹, V. Savinov¹³², G. Schnell¹³³, C. Schwanda¹³⁴, Y. Seino¹³⁵, K. Senyo¹³⁶, M. E. Seviror¹³⁷, W. Shan¹³⁸, C. Sharma¹³⁹, J.-G. Shiu¹⁴⁰, A. Sokolov¹⁴¹, E. Solovieva¹⁴², M. Starič¹⁴³, Z. S. Stottler¹⁴⁴, M. Sumihama¹⁴⁵, M. Takizawa¹⁴⁶, K. Tanida¹⁴⁷, F. Tenchini¹⁴⁸, R. Tiwary¹⁴⁹, T. Uglov¹⁵⁰, Y. Unno¹⁵¹, S. Uno¹⁵², Y. Usov¹⁵³, A. Vinokurova¹⁵⁴, M.-Z. Wang¹⁵⁵, S. Watanuki¹⁵⁶, E. Won¹⁵⁷, B. D. Yabsley¹⁵⁸, W. Yan¹⁵⁹, J. Yelton¹⁶⁰, J. H. Yin¹⁶¹, L. Yuan¹⁶², Z. P. Zhang¹⁶³, V. Zhilich¹⁶⁴, and V. Zhukova¹⁶⁵

(Belle Collaboration)



(Received 7 December 2023; accepted 21 February 2024; published 15 March 2024)

Using the full data sample of 980 fb^{-1} collected with the Belle detector at the KEKB asymmetric energy electron-positron collider, we report the results of the first search for the rare semileptonic decays $\Xi_c^0 \rightarrow \Xi^0 \ell^+ \ell^-$ ($\ell = e$ or μ). No significant signals are observed in the $\Xi^0 \ell^+ \ell^-$ invariant-mass distributions. Taking the decay $\Xi_c^0 \rightarrow \Xi^- \pi^+$ as the normalization mode, we report 90% credibility upper limits on the branching fraction ratios $\mathcal{B}(\Xi_c^0 \rightarrow \Xi^0 e^+ e^-)/\mathcal{B}(\Xi_c^0 \rightarrow \Xi^- \pi^+) < 6.7 \times 10^{-3}$ and $\mathcal{B}(\Xi_c^0 \rightarrow \Xi^0 \mu^+ \mu^-)/\mathcal{B}(\Xi_c^0 \rightarrow \Xi^- \pi^+) < 4.3 \times 10^{-3}$ based on the phase-space assumption for signal decays. The 90% credibility upper limits on the absolute branching fractions of $\mathcal{B}(\Xi_c^0 \rightarrow \Xi^0 e^+ e^-)$ and $\mathcal{B}(\Xi_c^0 \rightarrow \Xi^0 \mu^+ \mu^-)$ are found to be 9.9×10^{-5} and 6.5×10^{-5} , respectively.

DOI: 10.1103/PhysRevD.109.052003

I. INTRODUCTION

In the Standard Model (SM), the weak-current interaction has an identical coupling to all lepton generations, which allows Lepton Flavor Universality (LFU) to be tested in the semileptonic decays of the hadrons. Theoretically, the study of semileptonic decays of baryons has complications that are not present in the study of analogous decays of mesons as the contributions from W -exchange transitions lead to sensitivity to the helicity structure of the

effective Hamiltonian [1–4]. Furthermore, the hadronic form factors are not as well known for baryons as they are for mesons. Thus, the experimental results on baryonic semileptonic decays give important inputs for lattice quantum chromodynamics and other theoretical models.

Experimentally, few baryonic neutrinoless semileptonic decays have been observed. Of the light-baryon octet and bottom baryon decays, the branching fractions for $\Xi^0 \rightarrow \Lambda^0 e^+ e^-$, $\Sigma^+ \rightarrow p \mu^+ \mu^-$, and $\Lambda_b \rightarrow \Lambda \mu^+ \mu^-$ have been measured [5–9]. However, no evidence has been found for similar decays of charmed baryons. Among these decays, only $\Lambda_c^+ \rightarrow p \ell^+ \ell^-$ ($\ell = e$ or μ) decays were searched for. Upper limits on the branching fractions, at 90% credibility, were first set by the BABAR collaboration at $\mathcal{B}(\Lambda_c^+ \rightarrow p e^+ e^-) < 5.5 \times 10^{-6}$ and $\mathcal{B}(\Lambda_c^+ \rightarrow p \mu^+ \mu^-) < 44 \times 10^{-6}$

Published by the American Physical Society under the terms of the [Creative Commons Attribution 4.0 International license](https://creativecommons.org/licenses/by/4.0/). Further distribution of this work must maintain attribution to the author(s) and the published article's title, journal citation, and DOI. Funded by SCOAP³.

[10]. LHCb then placed a much tighter limit, at the 90% confidence level, on $\mathcal{B}(\Lambda_c^+ \rightarrow p\mu^+\mu^-)$ at 7.7×10^{-8} [11]. Particularly, the $\Lambda_c^+ \rightarrow p\ell^+\ell^-$ decays receive both single-quark transition via the Flavor Changing Neutral Current (FCNC) process and W -exchange contributions.

FCNC processes are forbidden at tree level in the SM, while the loop contributions are suppressed by the Glashow-Iliopoulos-Maiani mechanism [12]. However, some tensions have been reported recently in B meson decays involving the $b \rightarrow s\ell^+\ell^-$ processes via LFU observables and angular analysis [13–18], whereas recently LHCb reported the disappearance of the anomaly on LFU [19]. Hence, the study of semileptonic decays of baryons provides an opportunity to test the SM, and also can help in the understanding of the recent anomalies in meson FCNC processes.

The lack of studies on semileptonic decays of charmed baryons provides a strong motivation for further research on these decays. The $\Xi_c^0 \rightarrow \Xi^0\ell^+\ell^-$ decays, which are related to the W -exchange contribution in $\Lambda_c^+ \rightarrow p\ell^+\ell^-$ decays under SU(3) flavor symmetry, have not been experimentally measured yet. Measurement of both $\Xi_c^0 \rightarrow \Xi^0 e^+e^-$ and $\Xi_c^0 \rightarrow \Xi^0\mu^+\mu^-$ decay rates would also allow an LFU test to be performed. Based on the SU(3) flavor symmetry and the recent experimental result on $\mathcal{B}(\Lambda_c^+ \rightarrow p\mu^+\mu^-)$ [11], the upper limits at the 68.3% confidence level on the branching fractions of the Cabibbo-favored modes $\Xi_c^0 \rightarrow \Xi^0\ell^+\ell^-$ are predicted to be $\mathcal{B}(\Xi_c^0 \rightarrow \Xi^0 e^+e^-) < 2.35 \times 10^{-6}$ and $\mathcal{B}(\Xi_c^0 \rightarrow \Xi^0\mu^+\mu^-) < 2.25 \times 10^{-6}$ [1].

In this paper, we show the results of the first search for the $\Xi_c^0 \rightarrow \Xi^0\ell^+\ell^-$ decays, with $\Xi^0 \rightarrow \Lambda\pi^0$, $\Lambda \rightarrow p\pi^-$, using the full data sample of 980 fb^{-1} collected with the Belle detector [20]. The decay $\Xi_c^0 \rightarrow \Xi^-\pi^+$, $\Xi^- \rightarrow \Lambda\pi^-$, $\Lambda \rightarrow p\pi^-$ is used as the normalization mode.

II. THE DATA SAMPLE AND THE BELLE DETECTOR

This analysis is based on data recorded at or near the $\Upsilon(nS)$ ($n = 1-5$) resonances by the Belle detector [20] at the KEKB asymmetric energy electron-positron collider [21]. The Belle detector is a large solid-angle magnetic spectrometer consisting of a silicon vertex detector, a 50-layer central drift chamber (CDC), an array of aerogel threshold Cherenkov counters (ACC), a barrel-like arrangement of time-of-flight scintillation counters (TOF), an electromagnetic calorimeter (ECL) comprised of CsI(Tl) crystals located inside a superconducting solenoid coil that provides a 1.5 T magnetic field, and an iron flux return placed outside the coil, which is instrumented to detect K_L^0 mesons and to identify muons (KLM).

Signal Monte Carlo (MC) events are generated using EvtGen [22] to determine signal shapes, optimize the selection criteria, and calculate the reconstruction efficiencies. The generated $e^+e^- \rightarrow c\bar{c}$ events are simulated using

PYTHIA [23] with a specific Belle configuration. The Ξ_c^0 particles in signal MC simulation decay to $\Xi^0 e^+e^-$, $\Xi^0\mu^+\mu^-$, and $\Xi^-\pi^+$ using a phase-space model. These events are processed by a detector simulation based on Geant3 [24]. The Belle generic MC samples, which contain the MC samples of $\Upsilon(1S, 2S, 3S)$ decays, $\Upsilon(4S) \rightarrow B^+B^-/B^0\bar{B}^0$, $\Upsilon(5S) \rightarrow B_s^{(*)}\bar{B}_s^{(*)}$, and $e^+e^- \rightarrow q\bar{q}$ ($q = u, d, s, c$) at center-of-mass (c.m.) energies, \sqrt{s} , of 9.46, 10.024, 10.355, 10.52, 10.58, and 10.867 GeV with 2 times the total integrated luminosity of data, are used to study possible peaking backgrounds and verify the event selection criteria.

III. EVENT SELECTION CRITERIA

For well-reconstructed charged tracks, except those from $\Xi^- \rightarrow \Lambda\pi^-$ and $\Lambda \rightarrow p\pi^-$ decays, the impact parameters perpendicular to and along the beam direction with respect to the nominal interaction point (IP) are required to be less than 0.1 cm and 2 cm, respectively. Particle identification (PID) is applied to the reconstructed tracks. Pions, kaons, and protons are distinguished based on specific ionization in the CDC, time measurement in the TOF, and the response of the ACC: this information is combined to form a likelihood \mathcal{L}_i for each particle hypothesis i , where $i = \pi, K, \text{ or } p$. Related likelihoods are used to identify leptons: electron identification also includes a comparison of track and ECL cluster information, and muon identification is based on an extrapolation of the particle track, and hits in the KLM [25–27].

The Λ candidates are reconstructed via $\Lambda \rightarrow p\pi^-$ decay using a Kalman filter [28] with fitted χ^2 probability, P_{χ^2} , greater than 0. The reconstructed mass should be within $\pm 3.5 \text{ MeV}/c^2$ of the nominal mass [29], corresponding to approximately 2.5 times of the mass resolution (σ). The transverse distance for the reconstructed Λ vertex with respect to the IP is required to be greater than 0.35 cm. A loose PID requirement is applied on the proton with $\mathcal{L}_p/(\mathcal{L}_p + \mathcal{L}_K) > 0.2$ and $\mathcal{L}_p/(\mathcal{L}_p + \mathcal{L}_\pi) > 0.2$. In addition $\cos(\alpha_{xyz}(\Lambda))$ is required to be larger than 0. Hereinafter, $\alpha_{xyz}(i)$ is defined as the angle between the vector from the IP to the fitted decay vertex and the momentum vector of the reconstructed particle i ; $\alpha_{xy}(i)$ is defined as the angle between the projections of these vectors on the plane perpendicular to the beam direction.

Each π^0 candidate is reconstructed from a pair of photons with energy larger than 30 MeV in the barrel region of the ECL ($-0.63 < \cos\theta < 0.85$) or larger than 50 MeV in the endcaps ($-0.91 < \cos\theta < -0.63$ or $0.85 < \cos\theta < 0.98$). Here, θ is the polar angle with respect to the detector axis, with the $\theta = 0$ direction aligned approximately with the e^- beam. The reconstructed invariant mass of the π^0 candidates is required to be within $\pm 17.4 \text{ MeV}/c^2$ ($\sim 3\sigma$) of the π^0 nominal mass. A mass-constrained fit is applied to the π^0

candidates, and the momenta of the fitted π^0 candidates in the laboratory frame are required to exceed 0.15 GeV/c.

The $\Xi^- \rightarrow \Lambda \pi^-$ decays are selected using the following criteria. The π^- track is required to have a transverse momentum higher than 50 MeV/c. A TreeFit algorithm [28] which performs global decay chain vertex fitting for a particular process has been applied to the Ξ^- decay chain with $P_{\chi^2} > 0$ required. The decay chain is required to satisfy $\cos(\alpha_{xyz}(\Xi^-)) > 0$ and $\cos(\alpha_{xy}(\Lambda))/\cos(\alpha_{xy}(\Xi^-)) < 1.006$. The distances of the decay vertices of the reconstructed candidates from the IP, denoted as L_i , should satisfy $L_\Lambda > L_{\Xi^-} > 0.1$ cm. The reconstructed mass should be within ± 5 MeV/c² ($\sim 2.5\sigma$) of the nominal mass [29].

The Ξ^0 is reconstructed by combining the selected Λ and π^0 candidates. A TreeFit [28,30] to the Ξ^0 decay chain is applied with $P_{\chi^2} > 0$ required. Since the π^0 from Ξ^0 decay has negligible vertex position information, the fit is performed with the following steps. Firstly, taking the IP as the point of origin of the Ξ^0 , the point of intersection of the Ξ^0 trajectory and the reconstructed Λ trajectory is found. Then, this position is taken as the decay location of the Ξ^0 hyperon, and the π^0 is then remade using this position as its point of origin. Only those combinations with the decay location of the Ξ^0 indicating a positive Ξ^0 path length are retained. The decay chain is also required to satisfy $\cos(\alpha_{xyz}(\Xi^0)) > 0$, $\cos(\alpha_{xy}(\Xi^0)) > \cos(\alpha_{xy}(\Lambda))$, and $L_\Lambda > L_{\Xi^0} > 0.5$ cm. The reconstructed mass should be within ± 12 MeV/c² ($\sim 2.5\sigma$) of the nominal mass. This procedure follows that presented in Ref. [31], and gives a Ξ^0 signal yield of approximately 6.4×10^5 according to the fit to the $M(\Lambda\pi^0)$ distribution shown in Ref. [31]. Backgrounds are studied using sideband samples: Ξ^0 candidates whose invariant mass differs by between 20 and 44 MeV/c² from the nominal value [29].

For the normalization channel $\Xi_c^0 \rightarrow \Xi^- \pi^+$, the selected Ξ^- hyperons are combined with selected π^+ candidates identified with $\mathcal{L}_\pi/(\mathcal{L}_\pi + \mathcal{L}_K) > 0.2$ and $\mathcal{L}_\pi/(\mathcal{L}_\pi + \mathcal{L}_p) > 0.2$. To reconstruct the signal modes $\Xi_c^0 \rightarrow \Xi^0 \ell^+ \ell^-$, the Ξ^0 candidate is combined with a pair of lepton tracks, $e^+ e^-$ or $\mu^+ \mu^-$, which are identified with $\mathcal{L}_e/(\mathcal{L}_e + \mathcal{L}_{\text{non-}e}) > 0.9$ and $\mathcal{L}_\mu/(\mathcal{L}_\mu + \mathcal{L}_K + \mathcal{L}_\pi) > 0.9$ for electrons and muons, respectively, where $\mathcal{L}_{\text{non-}e}$ is the likelihood for non-electron tracks. The Ξ_c^0 candidates should be consistent with originating from the IP and pass the vertex and mass-constrained fits with $P_{\chi^2} > 0.01$ to the whole decay chain including the intermediate states, Ξ^0 , Ξ^- , Λ , and π^0 [28]. To reduce combinatorial background, especially those from B meson decays, the scaled momentum for the Ξ_c^0 candidate, $x_p = p_{\Xi_c^0}^* c / \sqrt{s/4 - M_{\Xi_c^0}^2 c^4}$, is required to be greater than 0.5, where $p_{\Xi_c^0}^*$ is the momentum of Ξ_c^0 candidate in the $e^+ e^-$ c.m. frame and $M_{\Xi_c^0}$ is the invariant mass of the Ξ_c^0 candidate. To suppress background from photon conversion for

$\Xi_c^0 \rightarrow \Xi^0 e^+ e^-$ decay, the $e^+ e^-$ pair is required to have invariant mass greater than 0.1 GeV/c². Each of the electron candidates is also combined with every opposite-charged particle in the event, using the electron hypothesis: the invariant mass of all such pairs is required to be greater than 0.1 GeV/c². In events where there is at least one candidate, the average number of candidates is about 1.3. All candidates are retained.

The selection criteria on the invariant mass of the electron pair, P_{χ^2} for the Ξ_c^0 decay chain, and scaled momentum x_p in this analysis are optimized by maximizing the Punzi figure of merit, $\varepsilon/(3/2 + \sqrt{B})$ [32]. Here, “3” is the desired significance level, ε is the detection efficiency of the $\Xi_c^0 \rightarrow \Xi^0 e^+ e^-$ mode based on signal MC simulation, and B is the number of the normalized generic MC events in the signal range, $2.32 < M_{\Xi^0 e^+ e^-} < 2.50$ GeV/c² ($> 95\%$ signal events retained). These requirements are also found to be optimal for $\Xi_c^0 \rightarrow \Xi^0 \mu^+ \mu^-$, so they are applied for both channels.

IV. BRANCHING FRACTION MEASUREMENT

For the reference mode, $\Xi_c^0 \rightarrow \Xi^- \pi^+$, the above selection criteria for Ξ^- and Ξ_c^0 candidates are applied. Figure 1 shows the invariant-mass distribution of $\Xi^- \pi^+$ combinations from data, together with the result of an unbinned extended maximum-likelihood (EML) fit. In the fit, the signal shape of the Ξ_c^0 candidates is parametrized by a double-Gaussian function, and the background shape is described by a first-order polynomial. The fit parameters are left free yielding a Ξ_c^0 mass consistent with known values [29]. The fitted signal yield is 28937 ± 272 .

After applying the selection criteria introduced in the last section, for the reconstructed candidates, the $\Xi^0 \ell^+ \ell^-$ mass is evaluated and either mass is required to be in the range (2.32 ~ 2.50) GeV/c². The corresponding Ξ^0 invariant mass is shown in Fig. 2. A small Ξ^0 contribution to these events can be seen. To estimate it we perform a fit with a double-Gaussian function to model the signal shape, and a

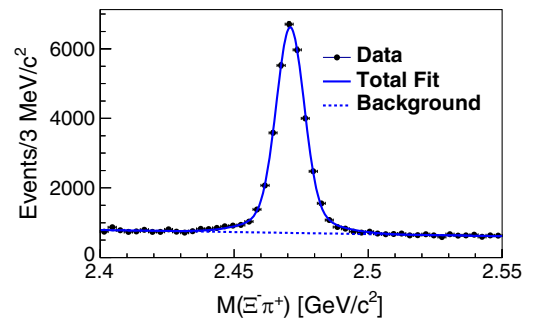


FIG. 1. The invariant-mass distribution of $\Xi^- \pi^+$ combinations in data. The dots with error bars represent the data, the solid curve shows the best-fit result, and the blue dashed curve shows the fitted backgrounds.

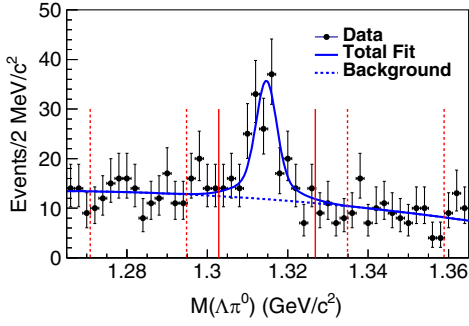


FIG. 2. The invariant-mass distributions of $\Xi^0 \rightarrow \Lambda\pi^0$ candidates from the selected $\Xi^0 \ell^+ \ell^-$ candidates with $2.32 < M_{\Xi^0 \ell^+ \ell^-} < 2.50$ GeV/c^2 in the data together with the fit results. The dots with error bars represent the data, the solid curve shows the total best-fit result, the dashed curve shows the background shape, and the solid and dashed lines show the signal and sideband regions of Ξ^0 candidates, respectively.

second-order polynomial to model the background. The signal shape parameters are fixed to the values found in signal MC, while the background parameters are free in the fit. The fitted Ξ^0 signal yield is 95.7 ± 15.6 .

The invariant-mass distributions of $\Xi^0 e^+ e^-$ and $\Xi^0 \mu^+ \mu^-$ from signal MC simulations and data are shown in Figs. 3

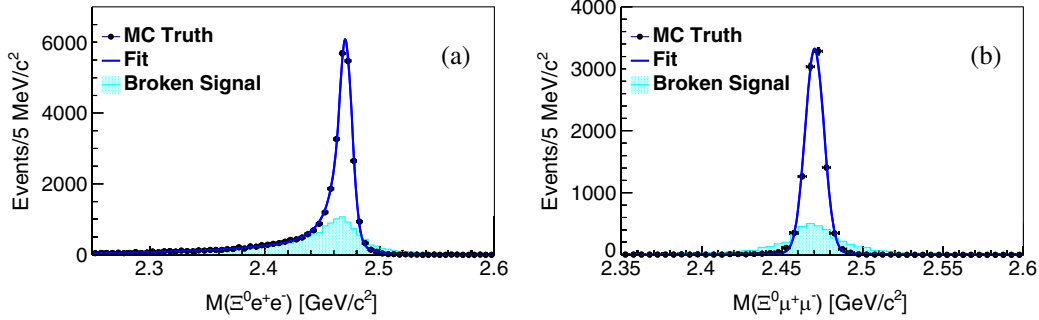


FIG. 3. The invariant-mass distributions of (a) $\Xi^0 e^+ e^-$ and (b) $\Xi^0 \mu^+ \mu^-$ combinations in signal MC simulation. Points with error bars show the correctly reconstructed signal, the blue solid curves show the results of the fit to the signal shape, and the cyan shaded histograms show the broken signal distributions.

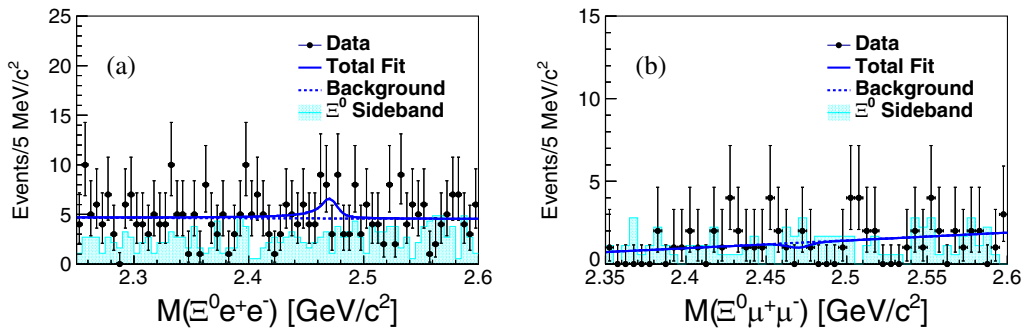


FIG. 4. The invariant-mass distributions of (a) $\Xi^0 e^+ e^-$ and (b) $\Xi^0 \mu^+ \mu^-$ combinations in data. Points with error bars show the data, the solid curves show the best-fit results, and the blue dashed curves show the background component in the fits. Cyan shaded histograms show the normalized $\Lambda\pi^0 \ell^+ \ell^-$ mass spectrum for the $\Lambda\pi^0$ mass in the Ξ^0 sidebands.

and 4, respectively, together with the unbinned EML fit results to the true signal distributions from signal MC events and spectra from data. To take energy loss due to bremsstrahlung into account, the shapes of correctly reconstructed Ξ_c^0 candidates are described by two Crystal Ball functions [33] for the dielectron mode, while a double-Gaussian function is used as the signal shape for the dimuon mode. Incorrectly reconstructed signal candidates (“broken signal”) have a broader distribution in signal MC simulation, shown by the cyan-shaded histograms in Fig. 3. A broken signal is mainly due to incorrectly selected photons in Ξ^0 reconstruction. Similar to the treatment in Ref. [34], we extract the shape of the broken signal from MC simulation via rookeyspdf [35], and treat it as a distinct component in the final Ξ_c^0 signal yield extraction. The peaking background components are determined using the algorithm of Ref. [36], and we find them to be negligible.

No significant $\Xi_c^0 \rightarrow \Xi^0 \ell^+ \ell^-$ signals are observed in the data. The cyan shaded histograms in Fig. 4 show the normalized $\Lambda\pi^0 \ell^+ \ell^-$ mass spectrum for the $\Lambda\pi^0$ mass in the Ξ^0 sidebands, and provide an estimate of the contribution from $\Lambda\pi^0$ combinatorial background in Ξ^0 reconstruction. This is the largest contribution to the background. The small excess in data above the normalized sidebands is

consistent with a small contribution from true $\Xi^0 \rightarrow \Lambda \pi^0$ decays (see Fig. 2), combined with unrelated $\ell^+ \ell^-$ candidates. For the fits to data, the signal shapes are taken from the fits to the signal MC samples above with all the parameters fixed. Here, the width of the signal shape is multiplied by a correction factor $R_\sigma = \sigma_{\text{data}}/\sigma_{\text{MC}} = 1.12 \pm 0.06$, where σ_{data} and σ_{MC} are the fitted resolutions of $\Xi_c^0 \rightarrow \Xi^- \pi^+$ shapes from data and MC simulation, respectively. The broken signal shape is taken from the MC simulation as described above, and the ratio of the broken signal to correctly reconstructed signal events, $R_{\text{broken/signal}}$, is fixed at 0.50 (0.46) for the $\Xi^0 e^+ e^-$ ($\Xi^0 \mu^+ \mu^-$) mode according to MC simulation. Linear functions with free parameters are used for the smooth background shapes. The fitted Ξ_c^0 signal yields are 9.1 ± 7.1 with a significance of 1.4σ and -0.9 ± 2.1 for $\Xi_c^0 \rightarrow \Xi^0 e^+ e^-$ and $\Xi_c^0 \rightarrow \Xi^0 \mu^+ \mu^-$ decays, respectively.

Assuming the signal branching fraction has a uniform prior probability density function, the Bayesian upper limit at 90% credibility on the number of signal events (N^{UL}) is determined by solving the equation $\int_0^{N^{\text{UL}}} \mathcal{L}(x) dx = 0.90 \int_0^\infty \mathcal{L}(x) dx$, where x is the number of fitted signal events and $\mathcal{L}(x)$ is the likelihood function in the fit to data. The upper limits at 90% credibility on the relative branching fractions are calculated by

$$\begin{aligned} & \mathcal{B}^{\text{UL}}(\Xi_c^0 \rightarrow \Xi^0 \ell^+ \ell^-) / \mathcal{B}(\Xi_c^0 \rightarrow \Xi^- \pi^+) \\ &= \frac{N^{\text{UL}}(\Xi_c^0 \rightarrow \Xi^0 \ell^+ \ell^-)}{N^{\text{obs}}(\Xi_c^0 \rightarrow \Xi^- \pi^+)} \times \frac{\varepsilon(\Xi_c^0 \rightarrow \Xi^- \pi^+)}{\varepsilon(\Xi_c^0 \rightarrow \Xi^0 \ell^+ \ell^-)} \\ & \times \frac{\mathcal{B}(\Xi^- \rightarrow \Lambda \pi^-)}{\mathcal{B}(\Xi^0 \rightarrow \Lambda \pi^0)}, \end{aligned} \quad (1)$$

separately for $\ell = e$ and $\ell = \mu$. Here, $N^{\text{UL}}(\Xi_c^0 \rightarrow \Xi^0 \ell^+ \ell^-)$ and $\varepsilon(\Xi_c^0 \rightarrow \Xi^0 \ell^+ \ell^-)$ are the upper limits on signal yield in data and the reconstruction efficiencies according to MC simulations, respectively, of $\Xi_c^0 \rightarrow \Xi^0 \ell^+ \ell^-$ decays, $N^{\text{obs}}(\Xi_c^0 \rightarrow \Xi^- \pi^+)$ and $\varepsilon(\Xi_c^0 \rightarrow \Xi^- \pi^+)$ are the number

TABLE I. The summarized values for branching fraction measurements of $\Xi_c^0 \rightarrow \Xi^0 \ell^+ \ell^-$ decays. Here, N^{fit} is the fitted signal yield, N^{UL} is the 90% credibility upper limit on the number of signal events from data before considering systematic uncertainties, $\mathcal{B}^{\text{UL}}/\mathcal{B}(\Xi_c^0 \rightarrow \Xi^- \pi^+)$ and \mathcal{B}^{UL} are the 90% credible upper limits on the relative and absolute branching fractions, respectively, for the $\Xi_c^0 \rightarrow \Xi^0 \ell^+ \ell^-$ decays with systematic uncertainties included, and $\mathcal{B}(\Xi_c^0 \rightarrow \Xi^- \pi^+) = (1.43 \pm 0.32)\%$ is taken from the Particle Data Group [29].

Modes	$\Xi_c^0 \rightarrow \Xi^0 e^+ e^-$	$\Xi_c^0 \rightarrow \Xi^0 \mu^+ \mu^-$
Efficiency (%)	1.58	0.53
N^{fit}	9.1 ± 7.1	-0.9 ± 2.1
N^{UL}	19.9	4.5
$\mathcal{B}^{\text{UL}}/\mathcal{B}(\Xi_c^0 \rightarrow \Xi^- \pi^+)$	6.7×10^{-3}	4.3×10^{-3}
\mathcal{B}^{UL}	9.9×10^{-5}	6.5×10^{-5}

of observed events in the data and the reconstruction efficiency, respectively, of $\Xi_c^0 \rightarrow \Xi^- \pi^+$ decay, and the branching fractions are taken as $\mathcal{B}(\Xi_c^0 \rightarrow \Xi^- \pi^+) = (1.43 \pm 0.32)\%$, $\mathcal{B}(\Xi^0 \rightarrow \Lambda \pi^0) = (99.524 \pm 0.012)\%$, and $\mathcal{B}(\Xi^- \rightarrow \Lambda \pi^-) = (99.887 \pm 0.035)\%$ [29]. To take into account the systematic uncertainties detailed in the next section, the likelihood curve is convolved with a Gaussian function whose width equals the corresponding total multiplicative systematic uncertainty. The calculated 90% credible upper limits on the numbers of signal events, and relative and absolute branching fractions in the data, are summarized in Table I. The muon identification criterion used in this analysis effectively excludes tracks with a momentum too low to reach the KLM [27]: this leads to a reconstruction efficiency in the dimuon channel that is a factor of 3 lower than in the dielectron channel.

V. SYSTEMATIC UNCERTAINTIES

The systematic uncertainties in the measurements of the branching fractions are divided into two categories: multiplicative and additive systematic uncertainties.

The sources of multiplicative systematic uncertainties include detection-efficiency-related uncertainties, branching fractions of intermediate states, and the fitting uncertainty for the normalization mode $\Xi_c^0 \rightarrow \Xi^- \pi^+$. The additive systematic uncertainties are the uncertainties in the fits to extract signal yields for $\Xi_c^0 \rightarrow \Xi^0 \ell^+ \ell^-$ decays.

The detection-efficiency-related uncertainties include those for tracking efficiency, PID efficiency, π^0 and Λ selection efficiencies, and are estimated based on the simulated MC samples. Since there are four charged tracks in the final states for both signal and reference decay modes, the uncertainty in tracking efficiency cancels in this analysis. The proton PID uncertainties are found to be 0.6% and 1.1% for $\Xi_c^0 \rightarrow \Xi^0 e^+ e^-$ and $\Xi_c^0 \rightarrow \Xi^0 \mu^+ \mu^-$ modes, respectively, by taking into account the proton momentum differences with the normalization mode. Since the $\Lambda \rightarrow p \pi^-$ decay is reconstructed in each decay mode and no PID requirement is assigned for the pion track decay from Λ , the other sources of Λ selection uncertainties cancel. Using the control samples of $D^{*+} \rightarrow D^0 \pi^+$ with $D^0 \rightarrow K^- \pi^+$, the PID uncertainties are estimated to be 0.5% and 0.6% for pions from Ξ_c^0 and Ξ^- decays, respectively, and are added linearly to be 1.1% for the pion tracks in $\Xi_c^0 \rightarrow \Xi^- \pi^+$ decay. Based on the study of $J/\psi \rightarrow \ell^+ \ell^-$ decay, the uncertainties from lepton identification are determined to be 3.2% for electrons and 5.2% for muons. The PID uncertainties here are summed in quadrature for different decay modes, assuming that those uncertainties are independent for $\Xi_c^0 \rightarrow \Xi^0 \ell^+ \ell^-$ and $\Xi_c^0 \rightarrow \Xi^- \pi^+$ decays. The total PID systematic uncertainties for $\Xi_c^0 \rightarrow \Xi^0 e^+ e^-$ and $\Xi_c^0 \rightarrow \Xi^0 \mu^+ \mu^-$ decays are determined to be 3.5% and 5.5%, respectively. The systematic uncertainties for momentum-weighted π^0 selection efficiency are estimated to be 3.3% and 3.0% for

TABLE II. The multiplicative systematic uncertainties (%) on the measurements of relative and absolute branching fractions.

Source	$\Xi_c^0 \rightarrow \Xi^0 e^+ e^-$	$\Xi_c^0 \rightarrow \Xi^0 \mu^+ \mu^-$
Particle ID	3.5	5.5
π^0 selection	3.3	3.0
$\mathcal{B}(\Xi_c^0 \rightarrow \Xi^- \pi^+)$	22.4	22.4
Fit of reference mode	0.7	0.7
Total [$\mathcal{B}(\Xi_c^0 \rightarrow \Xi^0 \ell^+ \ell^-)$]	4.9	6.3
Total [$\mathcal{B}(\Xi_c^0 \rightarrow \Xi^- \pi^+)$]	23.0	23.3

$\Xi_c^0 \rightarrow \Xi^0 e^+ e^-$ and $\Xi_c^0 \rightarrow \Xi^0 \mu^+ \mu^-$ decays, respectively, according to a study of a $\tau^- \rightarrow \pi^- \pi^0 \nu_\tau$ control sample. Assuming these uncertainties to be uncorrelated, the uncertainties from PID and π^0 efficiencies are added in quadrature to yield the total multiplicative systematic uncertainties.

For the measurements of ratios of branching fractions $\mathcal{B}^{\text{UL}}(\Xi_c^0 \rightarrow \Xi^0 \ell^+ \ell^-) / \mathcal{B}(\Xi_c^0 \rightarrow \Xi^- \pi^+)$, the uncertainties associated with branching fractions of intermediate states $\mathcal{B}(\Xi^- \rightarrow \Lambda \pi^-)$ and $\mathcal{B}(\Xi^0 \rightarrow \Lambda \pi^0)$ are 0.035% and 0.012% [29], respectively, which are negligible. In the measurements of absolute branching fractions, the uncertainty on

$\mathcal{B}(\Xi_c^0 \rightarrow \Xi^- \pi^+)$ is 22.4% [29], which is the dominant contribution.

In the fit to the $M(\Xi^- \pi^+)$ distribution from data for $\Xi_c^0 \rightarrow \Xi^- \pi^+$ decay, we change the fit range by $\pm 10\%$ and the order of the polynomial for the background shape, and the relative differences of the fitted signal yields are taken as the uncertainties. These uncertainties are added in quadrature: the total is 0.7%.

Additive systematic uncertainties due to the $\Xi^0 \ell^+ \ell^-$ invariant-mass fits are considered by reperforming the fits with all combinations of the following options: (1) change the resolution scale factor R_σ by $\pm 1\sigma$ of its uncertainty; (2) change the fit range by $\pm 10\%$, (3) change the polynomial describing the background shape from first order to second order; and (4) multiply the fixed $R_{\text{broken/signal}}$ ratios by the correction factors of 1.43 and 0.93 for wrong Ξ^0 combinations in dielectron and dimuon modes, respectively, which are calculated according to the ratios of the number of events in the normalized $\Lambda \pi^0 \ell^+ \ell^-$ mass spectrum for the $\Lambda \pi^0$ mass in the Ξ^0 sidebands from data over that from generic MC samples.

For the measurements of the upper limits at 90% credibility on the relative and absolute branching fractions

TABLE III. The detection efficiencies (%) in $(M_{e^+ e^-}^2, M_{\Xi^0 e^+}^2)$ bins for the $\Xi_c^0 \rightarrow \Xi^0 e^+ e^-$ decay mode.

$M_{e^+ e^-}^2$ (GeV ² /c ⁴)	$M_{\Xi^0 e^+}^2$ (GeV ² /c ⁴)						
	[1.4, 2.1]	[2.1, 2.8]	[2.8, 3.5]	[3.5, 4.2]	[4.2, 4.9]	[4.9, 5.6]	[5.6, 6.3]
[0, 0.15]	0.39 ± 0.01	0.98 ± 0.01	1.53 ± 0.01	1.69 ± 0.01	1.57 ± 0.01	1.03 ± 0.01	0.39 ± 0.01
[0.15, 0.3]	0.65 ± 0.01	1.20 ± 0.01	1.65 ± 0.01	1.78 ± 0.01	1.63 ± 0.01	1.08 ± 0.01	0.51 ± 0.01
[0.3, 0.45]	0.92 ± 0.01	1.32 ± 0.01	1.68 ± 0.01	1.78 ± 0.01	1.60 ± 0.01	1.06 ± 0.01	0.90 ± 0.03
[0.45, 0.6]	1.19 ± 0.01	1.48 ± 0.01	1.77 ± 0.01	1.83 ± 0.01	1.62 ± 0.01	1.15 ± 0.01	...
[0.6, 0.75]	1.30 ± 0.02	1.61 ± 0.01	1.87 ± 0.01	1.91 ± 0.01	1.63 ± 0.01	1.17 ± 0.01	...
[0.75, 0.9]	...	1.72 ± 0.01	1.97 ± 0.01	1.96 ± 0.01	1.56 ± 0.01	1.80 ± 0.07	...
[0.9, 1.05]	...	1.80 ± 0.01	2.07 ± 0.01	1.95 ± 0.01	1.53 ± 0.01
[1.05, 1.2]	...	1.75 ± 0.01	2.04 ± 0.01	1.81 ± 0.01	1.42 ± 0.02
[1.2, 1.35]	...	1.60 ± 0.02	1.78 ± 0.01	1.67 ± 0.01

TABLE IV. The detection efficiencies ($\times 10^{-3}$) in $(M_{\mu^+ \mu^-}^2, M_{\Xi^0 \mu^+}^2)$ bins for the $\Xi_c^0 \rightarrow \Xi^0 \mu^+ \mu^-$ decay mode.

$M_{\mu^+ \mu^-}^2$ (GeV ² /c ⁴)	$M_{\Xi^0 \mu^+}^2$ (GeV ² /c ⁴)				
	[2.1, 2.8]	[2.8, 3.5]	[3.5, 4.2]	[4.2, 4.9]	[4.9, 5.6]
[0, 0.15]	0.33 ± 0.01	5.87 ± 0.04	11.15 ± 0.05	6.66 ± 0.04	0.46 ± 0.01
[0.15, 0.3]	0.56 ± 0.01	6.68 ± 0.03	9.99 ± 0.04	6.01 ± 0.03	0.35 ± 0.01
[0.3, 0.45]	1.19 ± 0.01	7.05 ± 0.03	9.03 ± 0.04	5.38 ± 0.03	0.36 ± 0.01
[0.45, 0.6]	1.75 ± 0.02	7.05 ± 0.03	8.30 ± 0.03	4.60 ± 0.03	0.38 ± 0.01
[0.6, 0.75]	2.33 ± 0.02	7.11 ± 0.03	7.69 ± 0.03	3.82 ± 0.02	0.38 ± 0.02
[0.75, 0.9]	3.02 ± 0.02	6.92 ± 0.03	7.20 ± 0.03	3.38 ± 0.02	1.55 ± 0.40
[0.9, 1.05]	3.90 ± 0.03	6.84 ± 0.03	6.67 ± 0.03	3.60 ± 0.03	...
[1.05, 1.2]	5.24 ± 0.05	7.20 ± 0.03	6.59 ± 0.03	4.26 ± 0.11	...
[1.2, 1.35]	6.59 ± 0.16	7.87 ± 0.04	7.56 ± 0.06

of $\Xi_c^0 \rightarrow \Xi^0 \ell^+ \ell^-$ decays, the systematic uncertainties are taken into account in two steps. First, based on the study of the additive systematic uncertainties, the most conservative upper limits at 90% credibility on the numbers of Ξ_c^0 signal events are 25.6 and 4.6 for dielectron and dimuon modes, respectively. Then, the likelihood function of the case with the most conservative upper limit is convolved with a Gaussian function whose width equals the corresponding total multiplicative systematic uncertainty for each $\Xi_c^0 \rightarrow \Xi^0 \ell^+ \ell^-$ decay to get the final upper limit. The multiplicative systematic uncertainties from different sources are summarized in Table II.

In this analysis, the simulated $\Xi_c^0 \rightarrow \Xi^0 \ell^+ \ell^-$ decays are generated by the phase space model, since the exact physics models for the decays are unknown, and no significant signals are observed in data. Thus, no systematic uncertainty due to the choice of the decay model is included. Instead, we provide the reconstruction efficiencies in $(M_{\ell^+ \ell^-}^2, M_{\Xi^0 \ell^+}^2)$ bins, which are shown in Table III and Table IV for the dielectron and dimuon modes respectively.

VI. CONCLUSION

In summary, using the entire data sample of 980 fb^{-1} collected with the Belle detector, we search for the semi-leptonic decays $\Xi_c^0 \rightarrow \Xi^0 \ell^+ \ell^-$. No significant signals are observed in the $\Xi^0 \ell^+ \ell^-$ invariant-mass distributions. We determine 90% credible upper limits on the relative branching fraction ratios $\mathcal{B}(\Xi_c^0 \rightarrow \Xi^0 e^+ e^-)/\mathcal{B}(\Xi_c^0 \rightarrow \Xi^- \pi^+) < 6.7 \times 10^{-3}$ and $\mathcal{B}(\Xi_c^0 \rightarrow \Xi^0 \mu^+ \mu^-)/\mathcal{B}(\Xi_c^0 \rightarrow \Xi^- \pi^+) < 4.3 \times 10^{-3}$. Taking $\mathcal{B}(\Xi_c^0 \rightarrow \Xi^- \pi^+) = (1.43 \pm 0.32)\%$ [29], 90% credible upper limits on the absolute branching fractions $\mathcal{B}(\Xi_c^0 \rightarrow \Xi^0 e^+ e^-)$ and $\mathcal{B}(\Xi_c^0 \rightarrow \Xi^0 \mu^+ \mu^-)$ are determined to be 9.9×10^{-5} and 6.5×10^{-5} respectively.

Comparing with the theoretical predictions of the upper limits on the branching fractions of $\Xi_c^0 \rightarrow \Xi^0 \ell^+ \ell^-$ decays, $\mathcal{B}(\Xi_c^0 \rightarrow \Xi^0 e^+ e^-) < 2.35 \times 10^{-6}$ and $\mathcal{B}(\Xi_c^0 \rightarrow \Xi^0 \mu^+ \mu^-) < 2.25 \times 10^{-6}$ [1], the experimental upper limits reported in this paper using a uniform-phase-space distribution are higher by an order or magnitude compared with those calculated using theoretical arguments and input from other experimental results. A more precise analysis based on larger data samples collected by Belle II is expected in the future.

ACKNOWLEDGMENTS

This work, based on data collected using the Belle detector, which was operated until June 2010, was supported by the Ministry of Education, Culture, Sports, Science, and Technology (MEXT) of Japan, the Japan Society for the Promotion of Science (JSPS), and the Tau-Lepton Physics Research Center of Nagoya University; the Australian Research Council including Grants No. DP210101900, No. DP210102831, No. DE220100462, No. LE210100098,

and No. LE230100085; the Austrian Federal Ministry of Education, Science and Research (FWF) and FWF Austrian Science Fund No. P 31361-N36; National Key R&D Program of China under Contract No. 2022YFA1601903, National Natural Science Foundation of China and research Grants No. 11575017, No. 11761141009, No. 11705209, No. 11975076, No. 12135005, No. 12150004, No. 12161141008, and No. 12175041, and Shandong Provincial Natural Science Foundation Project ZR2022JQ02; the Czech Science Foundation Grant No. 22-18469S; Horizon 2020 ERC Advanced Grant No. 884719 and ERC Starting Grant No. 947006 ‘‘InterLeptons’’ (European Union); the Carl Zeiss Foundation, the Deutsche Forschungsgemeinschaft, the Excellence Cluster Universe, and the VolkswagenStiftung; the Department of Atomic Energy (Project Identification No. RTI 4002), the Department of Science and Technology of India, and the UPES (India) SEED finding programs No. UPES/R&D-SEED-INFRA/17052023/01 and No. UPES/R&D-SOE/20062022/06; the Istituto Nazionale di Fisica Nucleare of Italy; National Research Foundation (NRF) of Korea Grants No. 2016R1-D1A1B-02012900, No. 2018R1-A2B-3003643, No. 2018R1-A6A1A-06024970, No. RS-2022-00197659, No. 2019R1-I1A3A-01058933, No. 2021R1-A6A1A-03043957, No. 2021R1-F1A-1060423, No. 2021R1-F1A-1064008, and No. 2022R1-A2C-1003993; Radiation Science Research Institute, Foreign Large-size Research Facility Application Supporting project, the Global Science Experimental Data Hub Center of the Korea Institute of Science and Technology Information and KREONET/GLORIAD; the Polish Ministry of Science and Higher Education and the National Science Center; the Ministry of Science and Higher Education of the Russian Federation, Agreement 14.W03.31.0026, and the HSE University Basic Research Program, Moscow; University of Tabuk research Grants S-1440-0321, S-0256-1438, and S-0280-1439 (Saudi Arabia); the Slovenian Research Agency Grants No. J1-9124 and No. P1-0135; Ikerbasque, Basque Foundation for Science, and the State Agency for Research of the Spanish Ministry of Science and Innovation through Grant No. PID2022-136510NB-C33 (Spain); the Swiss National Science Foundation; the Ministry of Education and the National Science and Technology Council of Taiwan; and the United States Department of Energy and the National Science Foundation. These acknowledgements are not to be interpreted as an endorsement of any statement made by any of our institutes, funding agencies, governments, or their representatives. We thank the KEKB group for the excellent operation of the accelerator; the KEK cryogenics group for the efficient operation of the solenoid; and the KEK computer group and the Pacific Northwest National Laboratory (PNNL) Environmental Molecular Sciences Laboratory (EMSL) computing group for strong computing support; and the National Institute of Informatics, and Science Information NETwork 6 (SINET6) for valuable network support.

- [1] R. M. Wang, Y. G. Xu, C. Hua, and X. D. Cheng, *Phys. Rev. D* **103**, 013007 (2021).
- [2] Y.-M. Wang, Y. Li, and C.-D. Lü, *Eur. Phys. J. C* **59**, 861 (2009).
- [3] T. Mannel and S. Recksiegel, *J. Phys. G* **24**, 979 (1998).
- [4] G. Hiller, M. Knecht, F. Legger, and T. Schietinger, *Phys. Lett. B* **649**, 152 (2007).
- [5] J. R. Batley *et al.* (NA48 Collaboration), *Phys. Lett. B* **650**, 1 (2007).
- [6] H. Park *et al.* (HyperCP Collaboration), *Phys. Rev. Lett.* **94**, 021801 (2005).
- [7] T. Aaltonen *et al.* (CDF Collaboration), *Phys. Rev. Lett.* **107**, 201802 (2011).
- [8] R. Aaij *et al.* (LHCb Collaboration), *Phys. Lett. B* **725**, 25 (2013).
- [9] R. Aaij *et al.* (LHCb Collaboration), *J. High Energy Phys.* **06** (2015) 115.
- [10] J. P. Less *et al.* (BABAR Collaboration), *Phys. Rev. D* **84**, 072006 (2011).
- [11] R. Aaij *et al.* (LHCb Collaboration), *Phys. Rev. D* **97**, 091101 (2018).
- [12] S. Glashow, J. Iliopoulos, and L. Maiani, *Phys. Rev. D* **2**, 1285 (1970).
- [13] R. Aaij *et al.* (LHCb Collaboration), *Nat. Phys.* **18**, 277 (2022).
- [14] R. Aaij *et al.* (LHCb Collaboration), *Phys. Rev. Lett.* **122**, 191801 (2019).
- [15] R. Aaij *et al.* (LHCb Collaboration), *Phys. Rev. Lett.* **113**, 151601 (2014).
- [16] R. Aaij *et al.* (LHCb Collaboration), *J. High Energy Phys.* **08** (2017) 055.
- [17] R. Aaij *et al.* (LHCb Collaboration), *Phys. Rev. Lett.* **125**, 011802 (2020).
- [18] R. Aaij *et al.* (LHCb Collaboration), *Phys. Rev. Lett.* **126**, 161802 (2021).
- [19] R. Aaij *et al.* (LHCb Collaboration), *Phys. Rev. Lett.* **131**, 051803 (2023).
- [20] A. Abashian *et al.* (Belle Collaboration), *Nucl. Instrum. Methods Phys. Res., Sect. A* **479**, 422–117 (2002); also, see detector section in J. Brodzicka *et al.*, *Prog. Theor. Exp. Phys.* **2012**, 04D001 (2012).
- [21] S. Kurokawa and E. Kikutani, *Nucl. Instrum. Methods Phys. Res., Sect. A* **499**, 1 (2003), and other papers included in this volume; T. Abe *et al.*, *Prog. Theor. Exp. Phys.* **2013**, 03A001 (2013), and references therein.
- [22] D. J. Lange, *Nucl. Instrum. Methods Phys. Res. Sect. A* **462**, 152 (2001).
- [23] T. Sjöstrand, P. Edén, C. Friberg, L. Lönnblad, G. Miu, S. Mrenna, and E. Norrbin, *Comput. Phys. Commun.* **135**, 238 (2001).
- [24] R. Brun *et al.*, CERN Report No. DD/EE/84-1, 1984.
- [25] E. Nakano, *Nucl. Instrum. Methods Phys. Res., Sect. A* **494**, 402 (2002).
- [26] K. Hanagaki, H. Kakuno, H. Ikeda, T. Iijim, and T. Tsukamoto, *Nucl. Instrum. Methods Phys. Res., Sect. A* **485**, 490 (2002).
- [27] A. Abashian *et al.* (Belle Collaboration), *Nucl. Instrum. Methods Phys. Res., Sect. A* **491**, 69 (2002).
- [28] J.-F. Krohn *et al.*, *Nucl. Instrum. Methods Phys. Res., Sect. A* **976**, 164269 (2020).
- [29] R. L. Workman *et al.* (Particle Data Group), *Prog. Theor. Exp. Phys.* **2022**, 083C01 (2022).
- [30] J. Yelton *et al.* (Belle Collaboration), *Phys. Rev. D* **97**, 032001 (2018).
- [31] J. T. McNeil *et al.* (Belle Collaboration), *Phys. Rev. D* **103**, 112002 (2021).
- [32] G. Punzi, eConf C **MODT002**, 030908, 2003.
- [33] J. E. Gaiser, Ph.D. thesis, Stanford Linear Accelerator Center, Stanford University Report No. SLAC-R-255, 1982.
- [34] S. X. Li *et al.* (Belle Collaboration), *Phys. Rev. D* **107**, 032003 (2023).
- [35] K. S. Cranmer, *Comput. Phys. Commun.* **136**, 198 (2001).
- [36] X. Y. Zhou, S. X. Du, G. Li, and C. P. Shen, *Comput. Phys. Commun.* **258**, 107540 (2021).